Screening Current Induced Stress/Strain Analysis of High Field REBCO Coils With Co-Winding or Over-Banding Reinforcement

Yu Suetomi , Peng Xu , Ernesto S. Bosque , Andrey V. Gavrilin , W. Denis Markiewicz , Hongyu Bai , and Iain R. Dixon , *Senior Member, IEEE*

Abstract—Inclusion of screening current induced stress (SCIS) is becoming more commonplace in the design of ultra-high field magnets with REBCO tapes. It is desired to comprehensively manage tensile hoop stress, compressive hoop stress, and tilting angle caused by the SCIS. In this study, we have implemented effects of winding and cooldown processes to an already developed FEM model and analyzed the stress/strain behavior considering the SCIS on REBCO pancake coils in a 35 T LTS/HTS magnet with co-winding or over-banding reinforcement. Effects of thermal contraction and winding tension, and advantages/disadvantages of the co-winding or over-banding method are discussed.

Index Terms—Coupled mechanical and electromagnetic analysis, REBCO coil, screening current induced stress (SCIS), ultra-high field superconducting magnet.

I. INTRODUCTION

ONE of the major issues for an ultra-high field (UHF) magnet with REBCO tapes is the management of stress/strain inside REBCO coils. It is becoming more commonplace to include the effects of screening currents induced stress (SCIS), as seen in Fig. 1, during a design of REBCO insert coils [1], [2], [3], [4], [5], [6], [7], [8], [9], [10], [11], [12]. The SCIS leads to a tilting of REBCO tapes and a deformation of the coil into a dish-like shape (dishing). This results in excessive tensile hoop stress, potentially causing a waving deformation [13], [14] and compressive hoop stress can lead to a buckling deformation [4]. The impact of the tilting angle of REBCO tapes has not been clarified yet. Nevertheless, it is anticipated that a combination of significant axial compression forces and large tilting angles would lead to an increase in the tensile hoop stress. Therefore, it is essential not only to address tensile hoop stress but also
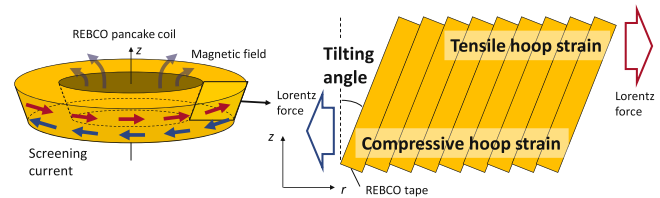
Fig. 1. Schematic of screening current induced stress (SCIS).
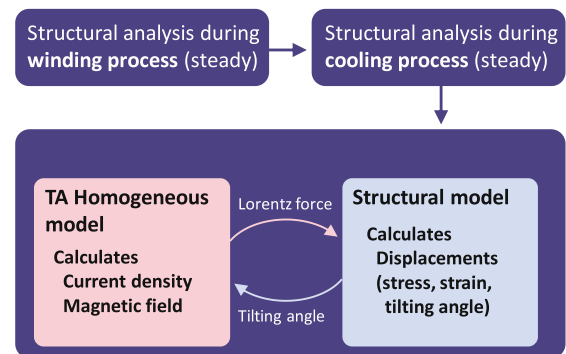
Fig. 2. Flow chart of the simulation method.

to consider compressive hoop stress and tilting angles. While co-winding and over-banding methods are commonly used as a reinforcement of an HTS coil in a UHF magnet, their effects on SCIS are only partially discussed in [6] and [7].

For precise estimation of stress/strain distribution considering SCIS, a sophisticated simulation model becomes essential. We have previously developed a 2D axisymmetric finite element method (FEM) model using the COMSOL Multiphysics, named 'FLOSSS' (Florida Screening Strain Software) [2].

In this study, we have enhanced the FLOSSS model by incorporating the influence of the winding and cooldown process for a more accurate simulation. The effects of these processes and co-winding/over-banding reinforcement on SCIS have been investigated.

II. NUMERICAL SIMULATION PROCEDURE

A. Simulation Method

Fig. 2 shows a simplified flow chart of the simulation method, developed with COMSOL Multiphysics. We apply steady state

TABLE I
PARAMETERS OF THE 35 T LTS/HTS MAGNET

Parameters	Unit	Co-winding (CW) option		Over-banding (OB) option	
		HTS1	HTS2	HTS1	HTS2
Inner radius; Outer radius	mm	20.0; 55.0	65.0; 110.5	20.0; 39.0	65.0; 89.7
Radial build; Number of turns per pancake	mm	35.0; 100	45.5; 130	19.0; 100	24.7; 130
Co-wound tape thickness; Over-band thickness	μm; μm	160.0; 0.0	160.0; 0.0	0.0; 160.0x100	0.0; 160.0x130
REBCO tape thickness; width	μm; mm	95x2; 4.1	95x2; 4.1	95x2; 4.1	95x2; 4.1
Reinforcement ratio		0.457	0.457	0.457	0.457
Number of double pancakes; Coil half height		24; 105.6	36; 158.4	24; 105.6	36; 158.4
Operating parameter					
Operating current I_{op}; Averaged current density[*]	A; A/mm^2	355; 231	355; 231	355; 425	355 425
B contribution for the center[**]	T	9.53	11.52	9.76	11.84
Magnitude and angle of B at the top pancake disk (innermost turn‑outermost turn)[**]	T; °	29‑24; 5‑9	20‑13; 15‑24	29‑24; 6‑9	20‑17; 17‑26
Range of I_{op}/I_c[**]	%	31‑60	16‑60	31‑60	15‑60

[*]Thickness of the co‑wound tape is included and that of the over‑banding is not included. [**]Calculated with uniform current density assumption.
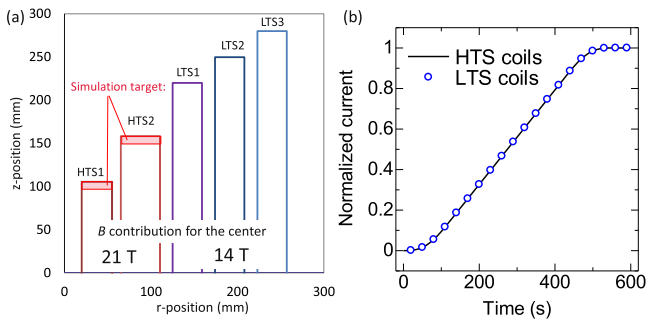
Fig. 3.   (a) Geometry of the 35 T LTS/HTS magnet. (b) Ramping profile of normalized operating current for HTS and LTS coils.

TABLE II
MECHANICAL PROPERTIES FOR THE STRUCTURAL ANALYSIS

Parameters	Unit	REBCO tape	SS tape	Ti-alloy
Young's modulus, E_r; E_θ; E_z	GPa	105; 143; 142	208 [17]	123 [19]
Coefficient of thermal contraction (293 K → to 4 K), α_r; α_θ; α_z	10^{-6}/K	9.79; 8.77; 8.78 [15], [16]	10.5 [18]	5.95 [19]

structural analysis for both the winding and cooling processes. This serves as a pre-process for the subsequent time-stepped coupled analysis during the charging process. Solutions of this pre-process are carried over to the next analysis process.

To analyze stress/strain distribution during the winding process, we employ the 'Birth and death method'. This method can analyze the effects of winding tension on the superconducting and reinforcement tapes and has been validated in [10].

In the time-stepped coupled analysis that simulates magnet charging, we use FLOSSS V2, the details of which are described in [2]. This couples the T-A electromagnetic analysis with the structural analysis. Notably, it incorporates the effects of the distributed tilting angle of the REBCO tape which significantly affects critical current and thus the SCIS [12].

The finite element model only considers the mandrel, REBCO tapes and co-winding or over-banding tapes. A displacement boundary condition is imposed along the bottom edge of the mandrel This constrains the displacement in the z-axis direction (u_z) to be zero. At the outward-inboard corner of each REBCO, co-winding, and over-banding turn, a roller corner condition is applied, constraining u_z to be zero. The interface between each structural element (mandrel to tape or tape to tape) is modeled by a frictionless contact, using a penalty method.

B. Simulation Target

As a simulation target of this study, a 35 T LTS/HTS hybrid magnet is presented only to show the effects of different design configurations; the magnet is not considered for construction.

Table I and Fig. 3(a) show parameters and geometries. To investigate suitable reinforcement methods, we designed a co-winding (CW) option and an over-banding (OB) option for the HTS inserts. In both options, a two-in-hand (two tapes bundled together) conductor is adopted along with stainless-steel (SS) tape as a reinforcement (co-winding or over-banding) material. The CW option has a co-winding SS tape with 160 μm thickness and no over-banding. The OB option has no co-winding materials and an over-banding with a total thickness of 16.0 mm (160 μm × 100 turns) and 20.8 mm (160 μm × 130 turns) for the inner HTS coil (HTS1) and the outer HTS coil (HTS2), respectively. Consequently, the reinforcement ratio over the winding of both options is identical, as seen in Table I. The mechanical parameters for the structural analysis are listed in Table II. The orthotropic properties of REBCO tape were calculated by using a mixture rule, incorporating in-house measurements for Young's modulus and data from references for the coefficient of thermal contraction [15], [16]. These designs do not contain insulation materials and a Ti-alloy is assumed for the mandrel material.

In this study, our focus was solely on the top pancake disks of the HTS1 and the HTS2. The coupling analysis, as shown in Fig. 2, was performed on these disks individually by employing a sub-modeling technique. The coupled analysis was not extended to the remaining pancake disks within the coil containing the pancake disk of interest, however, screening currents were computed using the T-A homogeneous model. In addition, a uniform current distribution was assumed in the other HTS and LTS coils.

The HTS coils and LTS coils are assumed to be simultaneously charged with an operating current (I_{op}) of 355 A and 268 A, respectively, as shown in Fig. 3(b). For simplicity, we assume that half of the I_{op} for HTS coils flows through each tape within a two-in-hand conductor.

We calculated the critical current (I_c) distribution utilizing (1) and parameters as shown in Table III. Here, B and θ_B are the magnitude of the magnetic field and its angle to the tape surface.
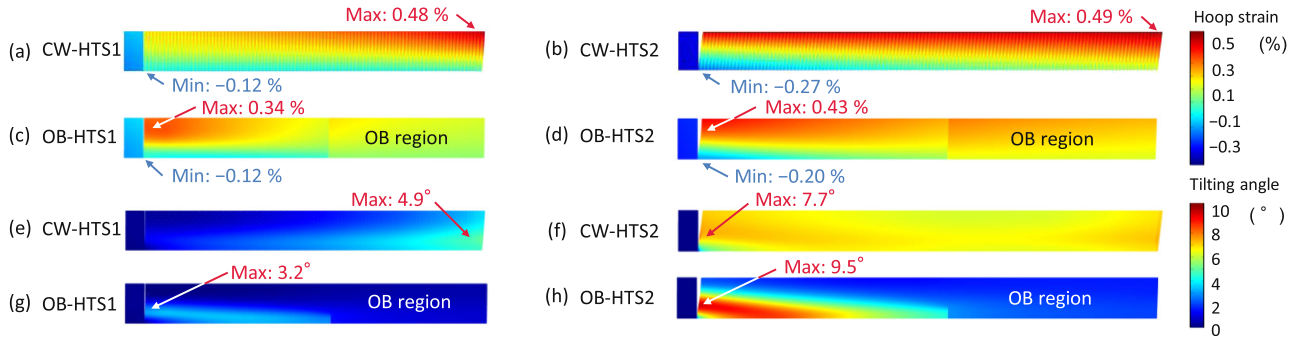
Fig. 4. Simulation results with the winding tension of 50 MPa at $t = 600$ s; Hoop strain distribution. (a) CW-HTS1. (b) CW-HTS2. (c) OB-HTS1. (d) OB-HTS2. Tilting angle distribution. (e) CW-HTS1. (f) CW-HTS2. (g) OB-HTS1. (h) OB-HTS2.

TABLE III
PARAMETERS FOR I_C CALCULATION

Parameters				
I_{c0}			2000	
k			0.063	
B_0			1.56	
α			1.088	
SF (Scaling factor)	0.612 (CW-HTS1)	0.883 (CW-HTS1)	0.923 (OB-HTS1)	0.946 (OB-HTS1)
γ_{ab} (ab-plane offset)			0.0	

This accounts for the tilting angle of the tape ($\theta_t = du/dz$) and ab-plane offset angle of the REBCO layer (γ_{ab}) as shown in (2) and (3). We set $\gamma_{ab} = 0$ in this calculation for simplicity.

$$I_c\left(B, \theta_B\right) = \frac{I_{C0}}{\left(1 + \frac{\sqrt{k^2 B_p^2 + B_n^2}}{B_0}\right)^\alpha} \cdot SF \quad (1)$$

$$B_p = B \cdot \cos\left(\theta_B - \theta_t - \gamma_{ab}\right) \quad (2)$$

$$B_n = B \cdot \sin\left(\theta_B - \theta_t - \gamma_{ab}\right) \quad (3)$$

The fraction of I_{op} to I_c (I_{op}/I_c) plays a significantly role in SCIS [1]. Given that the primary focus of this study is on the effects of reinforcement, we applied individual scaling factors (SF) for each coil option, adjusting the maximum I_{op}/I_c for the top pancake disks to 60%. The range of I_{op}/I_c over each coil is described in Table I.

The simulation was performed for the CW and OB options with/without thermal contraction and varying the winding tension to 0, 50 and 150 MPa. The same winding stress was applied to the REBCO, co-winding and over-banding tapes.

III. SIMULATION RESULTS AND DISCUSSIONS

A. Hoop Strain / Tilting Angle Distribution in CW or OB

Fig. 4 shows the distribution of hoop strain and tilting angle inside of the top pancake of HTS1 and HTS2 for the CW option (CW-HTS1 and CW-HTS2) and OB option (OB-HTS1 and OB-HTS2), at $t = 600$ s. The winding tension was set to 50 MPa. In all cases, positive hoop strain (tensile) and negative hoop strain (compressive) are generated at the outboard edge and the inboard edge, respectively. The inward Lorentz force generated on the lower half of the REBCO tapes tightens the

mandrel leading to the inward displacement of both the tapes and mandrel. This results in the generation of compressive hoop strain. The maximum compressive hoop strain occurs at the inboard edge of the innermost turn in all cases. The tilting angles are distributed along the tape width, indicating that the tapes experience bending in the tape width direction.

The maximum tensile hoop strain of CW-HTS1 and CW-HTS2 are 0.48% and 0.49%, respectively, occurring at the outboard edge of the outermost turn. In contrast, for the OB option, the location of the maximum hoop strain shifts towards the vicinity of the innermost turn. These values are 0.34% for OB-HTS1 and 0.43% for OB-HTS2, which are smaller than those of the CW option. This is attributed to the reinforcement provided by the over-band. However, the maximum tilting angle for OB-HTS2 is higher than that of CW-HTS2. Furthermore, there is a pronounced gradient in the tilting angle across the tape width in the OB-HTS2. This suggests that the OB option exhibits a greater tendency to bend in the tape width direction compared to the CW option. A more comprehensive comparison between CW and OB options is described in Section III-C.

B. Stress Distribution With/Without Thermal Contraction and With Various Winding Tension in CW or OB

Fig. 5 show distributions of radial stress along the centerline and hoop stress at the outboard edge of the top pancake disk in CW-HTS1, CW-HTS2, OB-HTS1 and OB-HTS2, with/without thermal contraction (TC) and with various winding tensions (WT). Additionally, plots of hoop stress calculated by $B_z J'_c R$ are provided in Fig. 5(c), (d), (g) and (h). Here, B_z and R represent magnetic field in the z-axis direction and radius, respectively. J'_c represents critical current density, defined as I_c divided by the area of the cross section of a turn including the REBCO tape and co-winding tape. B_z and J_c were extracted from the simulation results of "w/ TC, WT = 50 MPa", i.e., B_z was computed while considering the screening current distribution, and J_c was done while considering the tilting effect.

In the case of CW-HTS1, there is no radial compression, implying that there is no interaction between adjacent turns. The higher hoop stress is observed in the outer region of CW-HTS1. As indicated in [7], the maximum radially outward Lorentz force density should be estimated by J_c rather than ordinary average current density. Indeed, hoop stress on REBCO conductor in CW-HTS1 is in good agreement with the $B_z J'_c R$. The HTS1 tends to be in a state of no radial compression due to the distribution of large $B_z J'_c R$ in the outer region. On the other
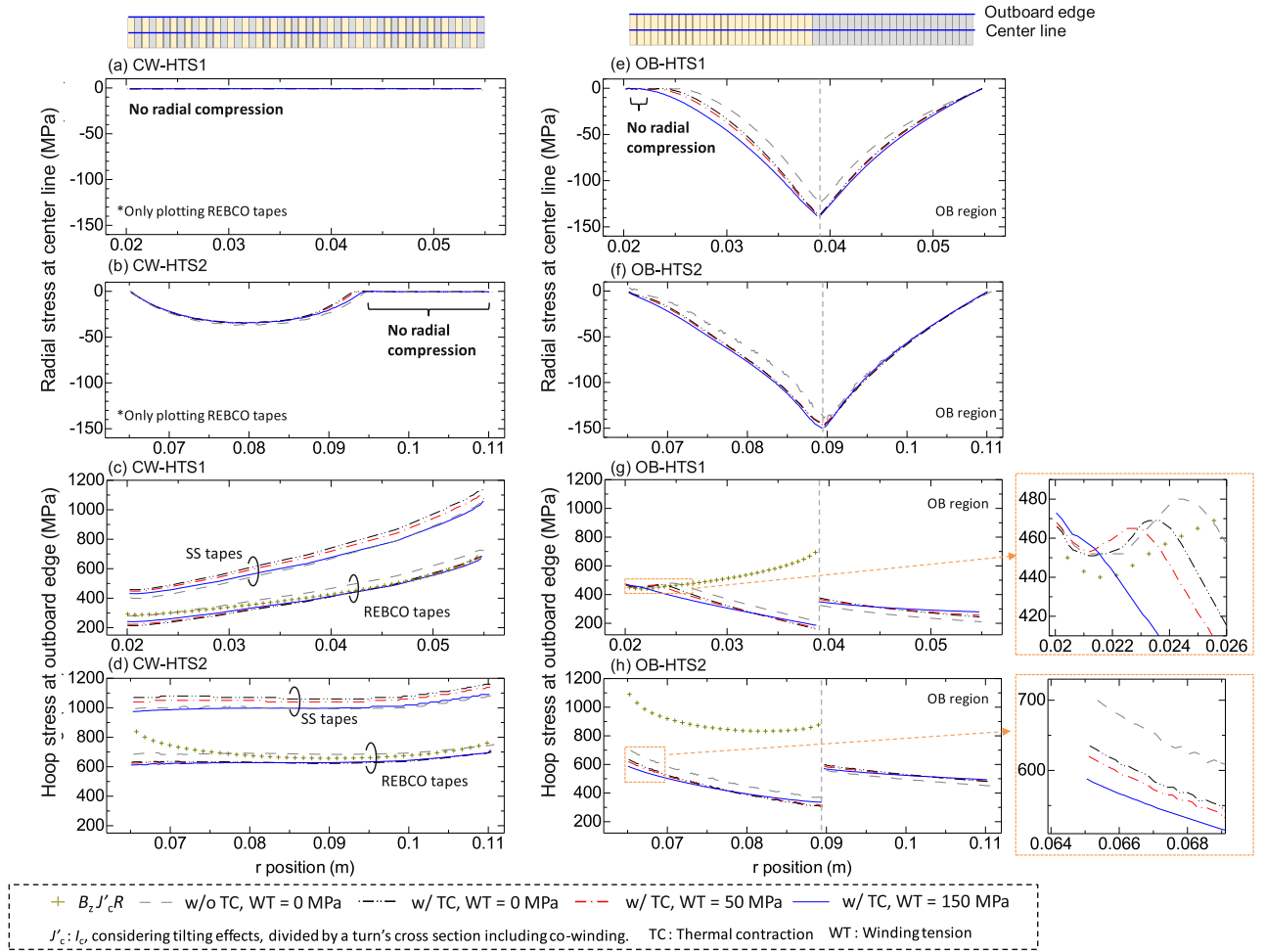
Fig. 5. Simulation results with/without thermal contraction (TC) and with various winding tension (WT) at $t = 600$ s; Radial stress distribution at the center line on the top pancake. (a) CW-HTS1. (b) CW-HTS2, (e) OB-HTS1. (f) OB-HTS2. Hoop stress distribution at the outboard edge on the top pancake. (c) CW-HTS1. (d) CW-HTS2. (g) OB-HTS1. (h) OB-HTS2.

hand, HTS2 shows gradual U-shaped distribution of $B_z J'_c R$, as seen in Fig. 5(d), which differs from the distribution of $B_z J'_c R$ in HTS1. This distribution contributes to the emergence of radial compression areas in over half of the winding pack in CW-HTS2.

In the case of the OB options, as seen in Fig. 5(e) and (f), almost all regions within HTS1 and HTS2 are under radial compression, and the hoop stress is reduced from $B_z J'_c R$ by the support provided by the over-band. However, regions of no radial compression remain only in the inner region of the OB-HTS1, and the hoop stress in these areas agrees with the $B_z J'_c R$.

1) *Limit of SCIS:* The hoop stress agrees well with the $B_z J'_c R$ in the case of the CW-HTS1 and the tilting angles for both CW and OB options are much lower than the magnetic field angle described in Table I. Therefore, SCIS was limited by the $B_z J'_c R$ rather than the magnetic field angle. This trend is different from what was described in [2], and it can be explained by the relatively low I_c of the simulated pancake disk in this study. The Lorentz force of $B_z J_c$ attempts to tilt the REBCO tape up to magnetic field angle, however, it is not sufficiently large to achieve this. Thus, the tilting angle does not reach the field angle and hoop stress is limited by $B_z J'_c R$.

2) *Effect of thermal contraction:* Fig. 5(c), (d), (g) and (h) show that the hoop stress on REBCO tape in the case of "w/ TC, WT = 0 MPa" is approximately 10% lower than that of "w/o TC, WT = 0 MPa". This reduction is attributed to the larger thermal contraction coefficient of SS tapes than that of REBCO tapes, as seen in Table II. The REBCO tapes experience compressive hoop stress derived from the contraction of the SS tapes.

3) *Effect of winding tension:* The typical stress state after winding is described in detail in [10]. Winding tension adds compressive radial and hoop stress to underlaying turns. The compressive stress increases along with the radial build. However, in the case of the CW option, the winding tension does not affect the hoop stress on the REBCO tapes after charging because it is not large enough to overcome the electro-magnetic loads. In the case of the OB-HTS1, while the winding tension slightly enlarges the radial compression areas, the no-radial compression area remains near the innermost region, and the peak hoop strain does not change, as seen in the inserted figure in the Fig. 5(g). In the case of the OB-HTS2, thanks to the radial compression over the entire winding pack, higher winding tension can reduce the maximum hoop
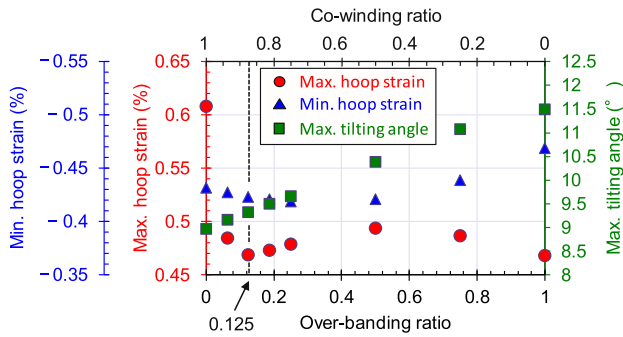
Fig. 6. Relationship between the CW ratio or the OB ratio and the maximum hoop strain, the minimum hoop strain and the maximum tilting angle.

Fig. 7. Simulation results on HTS2 with various OB ratio at $t = 600$ s. (a) Hoop strain distribution at the outboard edge. (b) Radial stress distribution at the center line.

TABLE IV
SUMMARY OF THE STRUCTURAL ANALYSIS

Parameters	Unit	HTS1		HTS2		CW:OB = 0.875:0.125
		CW	OB	CW	OB	
Max. hoop strain	%	0.52	0.43	0.54	0.47	0.46
Min. hoop strain	%	−0.24	−0.25	−0.40	−0.47	−0.39
Max. tilting angle	°	5.5	3.8	8.2	11.5	8.5
Ratio of radial compressive state	%	0	82	62	100	100

*Calculated with uniform current density assumption.

stress at the innermost turn. For example, the maximum hoop stress decreases from 635 MPa with WT = 0 MPa to 588 MPa with WT = 150 MPa. Thus, winding tension slightly suppresses the peak hoop stress on the REBCO tapes, especially in the case of OB-HTS2. However, the effect is not significant.

C. Co-winding vs. Over-banding

Here we discuss advantages and disadvantages of the CW and OB options. Table III shows the summary of the simulation results on the CW-HTS1, CW-HTS2, OB-HTS1 and OB-HTS2. The maximum and minimum values are extracted over the time domain. In most cases, the final state at $t = 600$ s does not show the maximum or minimum values because screening currents decrease after reaching the full-penetration state.

In the case of the HTS1, the OB option is suitable because of the lower tensile hoop strain and larger radial compression area. However, for HTS2, the OB option has advantages in terms of a lower tensile hoop strain and larger radial compression area, even though the CW option has benefits in terms of a lower degree of compressive hoop strain and tilting angle. Thus, there exists a trade-off relationship between the CW and OB reinforcement methods.

1) *Optimal distribution of CW and OB in HTS2:* Additional simulations were conducted by varying the co-winding ratio and over-banding ratio while keeping a constant reinforcement ratio over the winding of 0.457. For instance, in the case of a CW ratio : OB ratio = 0.5 : 0.5, the thickness of co-wound SS tape is 80 μm and the thickness of the over-band is 10.4 mm. Fig. 6 shows the relationship between the CW ratio or the OB ratio and the maximum hoop strain, the minimum hoop strain and the maximum tilting angle. The values were extracted at the maximum/minimum values in the time domain.

The maximum hoop strain drastically decreases with a slight increase in the OB ratio from 0, however this reduction becomes marginal when the OB ratio surpasses 0.125. Fig. 7 shows (a) the hoop strain distribution at the outboard edge and (b) the radial stress distribution at the center line of the HTS2 with OB ratio of 1.0, 0.25, 0.125 and 0.0. When the OB ratio is set to 0.125, the hoop strain distribution becomes relatively uniform, and the winding remains under radial compression. Therefore, it can be concluded that the optimal distribution is a CW ratio: OB ratio = 0.875 : 0.125, as it represents a balanced design when

compared to the singular CW or OB options. The summary of the simulation results is listed in Table IV.

IV. CONCLUSION

The code to simulate strain in REBCO coils has been enhanced to include the effects of winding tension and thermal contraction. This study investigated these effects and the effects of co-winding (CW) or over-banding (OB) reinforcement with considering SCIS on the REBCO pancake disk of inner coil (HTS1) and outer coil (HTS2) in a 35 T LTS/HTS magnet.

The REBCO coil with the CW option tends to have no radial compression inside of the winding pack, contrary to the OB option. This was observed to be more pronounced in insert coils, such as HTS1. Furthermore, it was found that SCIS is limited by the $B_z J'_c R$ rather than the field angle in the case of a coil with small J_c and large field angle. As a result of cooldown and thanks to larger thermal contraction coefficient of the SS tape than that of the REBCO tape, the maximum hoop stress on REBCO tape decreases by 10%. Regarding winding tension, a higher winding tension can reduce the peak hoop strain, especially in the OB-HTS2, thanks to it being in a radially compressive state over the entire winding pack. However, the effect is not significant. As a summary of simulation results, the OB option has the advantages of lower tensile hoop strain and larger radial compression area. On the other hand, the CW option has the advantages of lower compressive hoop strain and tilting angle. Thus, there is a tradeoff relationship between the CW and OB options. The combination of OB and CW is desired for HTS2, and we have found an optimal distribution of OB ratio and CW ratio.

It was found that by changing the distribution of the CW and OB, the tensile/compressive stress and tilting angle could be managed to some extent. In the future, it is desirable to establish criteria for these parameters that prevent coil damage and to develop design policy for an UHF magnet considering SCIS.

REFERENCES

[1] D. J. Kolb-bond et al., "Computing strains due to screening currents in REBCO magnets," *IEEE Trans. Appl. Supercond.*, vol. 30, no. 4, Jun. 2020, Art. no. 4602805.

[2] D. Kolb-Bond et al., "Screening current rotation effects: SCIF and strain in REBCO magnets," *Supercond. Sci. Technol.*, vol. 34, no. 9, 2021, Art. no. 095004, doi: 10.1088/1361-6668/ac1525.

[3] Y. Li et al., "Magnetization and screening current in an 800 MHz (18.8 T) REBCO nuclear magnetic resonance insert magnet: Experimental results and numerical analysis," *Supercond. Sci. Technol.*, vol. 32, no. 10, 2019, Art. no. 105007, doi: 10.1088/1361-6668/ab3119.

[4] S. Takahashi et al., "Hoop stress modification, stress hysteresis and degradation of a REBCO coil due to the screening current under external magnetic field cycling," *IEEE Trans. Appl. Supercond.*, vol. 30, no. 4, Jun. 2020, Art. no. 4602607, doi: 10.1109/TASC.2020.2974837.

[5] Y. Yan et al., "Screening current effect on the stress and strain distribution in REBCO high-field magnets: Experimental verification and numerical analysis," *Supercond. Sci. Technol.*, vol. 33, no. 5, 2020, Art. no. 05LT02, doi: 10.1088/1361-6668/ab7c52.

[6] Y. Yan et al., "Screening-current-induced mechanical strains in REBCO insert coils," *Supercond. Sci. Technol.*, vol. 34, no. 8, 2021, Art. no. 085012, doi: 10.1088/1361-6668/ac0b2d.

[7] Y. Yan, Y. Li, and T. Qu, "Screening current induced magnetic field and stress in ultra-high-field magnets using REBCO coated conductors," *Supercond. Sci. Technol.*, vol. 35, no. 1, 2022, Art. no. 014003, doi: 10.1088/1361-6668/ac392b.

[8] H. Ueda et al., "Numerical evaluation of the deformation of REBCO pancake coil, considering winding tension, thermal stress, and screening-current-induced stress," *Supercond. Sci. Technol.*, vol. 34, no. 2, 2021, Art. no. 024003, doi: 10.1088/1361-6668/abcd24.

[9] H. Ueda et al., "Experiment and numerical simulation of the combined effect of winding, cool-down, and screening current induced stresses in REBCO coils," *Supercond. Sci. Technol.*, vol. 35, no. 5, 2022, Art. no. 054001, doi: 10.1088/1361-6668/ac4b9e.

[10] M. Niu, J. Xia, and H. Yong, "Numerical analysis of the electromechanical behavior of high-field REBCO coils in all-superconducting magnets," *Supercond. Sci. Technol.*, vol. 34, no. 11, 2021, Art. no. 115005, doi: 10.1088/1361-6668/ac1a1f.

[11] S. Noguchi et al., "Electromagnetic behavior simulation of REBCO pancake coils considering REBCO tape rotation under high magnetic field," *IEEE Trans. Appl. Supercond.*, vol. 33, no. 5, Aug. 2023, Art. no. 4300405, doi: 10.1109/TASC.2023.3258372.

[12] Y. Li et al., "Screening-current-induced strain gradient on REBCO conductor: An experimental and analytical study with small coils wound with monofilament and striated multifilament REBCO tapes," *IEEE Trans. Appl. Supercond.*, vol. 30, no. 4, Jun. 2020, Art. no. 4702305, doi: 10.1109/TASC.2020.2974857.

[13] S. Hahn et al., "45.5-Tesla direct-current magnetic field generated with a high-temperature superconducting magnet," *Nature*, vol. 570, pp. 496–499, 2019, doi: 10.1038/s41586-019-1293-1.

[14] X. Hu et al., "Analyses of the plastic deformation of coated conductors deconstructed from ultra-high field test coils," *Supercond. Sci. Technol.*, vol. 33, no. 9, 2020, Art. no. 095012, doi: 10.1088/1361-6668/aba79d.

[15] *CryoComp*, Florence, SC, USA: Eckels Engineering.

[16] National Institute of Standards and Technology, "Material properties: OFHC copper (UNS C10100/C10200)," [Online]. Available: https://trc.nist.gov/cryogenics/materials/OFHC%20Copper/OFHC_Copper_rev1.htm

[17] N. J. Simon and R. P. Reed, *Structural Materials For Superconducting Magnets*. Boulder, CO, USA: National Bureau Standards, 1982.

[18] *Handbook On Materials for Superconducting Machinery*. Boulder, CO, USA: National Bureau Standards, 1977.

[19] P. Hidnert, *Thermal Expansion of Titanium*. Boulder, CO, USA: J. Res. National Bureau Standards, 1943.